Nuclear Physics **A405** (1983) 463–496
© North-Holland Publishing Company

LARGE-ANGLE PROTON EMISSION IN THE ^{9}Be(p, 2p) REACTION AT 300 MeV

R.E.L. GREEN, D.H. BOAL, R.L. HELMER, K.P. JACKSON and R.G. KORTELING

Simon Fraser University, Burnaby, BC, Canada V5A 1S6
and
TRIUMF, 4004 Wesbrook Mall, Vancouver, BC, Canada V6T 2A3

Received 28 February 1983

Abstract: A ^{9}Be(p, 2p) coincidence experiment performed to further elucidate the reaction mechanism for the production of energetic wide-angle protons in intermediate-energy proton-induced reactions is reported. Detectors in a coplanar geometry were used to measure coincidences between trigger protons at 90° to the beam and forward-angle protons on the opposite side of the beam. The incident proton energy was 300 MeV. We report both the inclusive spectra for the trigger protons and the differential mean multiplicities for the coincidence events.

The outgoing proton energies were measured using NaI detectors. Trigger protons were grouped into 10 MeV bins covering the kinetic energy range from 55 to 155 MeV. The forward protons were measured over a kinetic energy range of 65–280 MeV and an angular range of 14–60° with respect to the beam.

The present results are compared with two previous experiments which covered a more restrictive kinematical range. Calculations are performed with both phase-space and direct knockout models, and compared with experiment. Observation of angle and energy correlation effects suggested by knockout models indicate that such direct mechanisms provide a significant contribution to energetic wide-angle inclusive proton spectra.

E | NUCLEAR REACTIONS Be(p, pX), (p, 2pX), $E = 300$ MeV; measured $\sigma(E_p, \theta_p)$, $\sigma(E_1, \theta_1, E_2, \theta_2 = 90°)$, pp-coin. Comparison with phase-space and direct knockout calculations.

1. Introduction

The inclusive reactions of many different projectile-ejectile-target mass number combinations have been extensively studied in the last decade, particularly for ejectiles observed at wide angles and for projectiles with kinetic energies per nucleon in the 100 MeV to 2 GeV range. [For reviews, see refs. [1,2]).] What is striking about the energy spectra of the reaction products at fixed angle and at energies above the Coulomb barrier is that they are roughly exponential in shape, even with such widely different projectiles as electrons [3]) and heavy ions [1]) (with some exception for light ejectiles at forward angles). A rather large number of models have been advanced to explain these data, each involving differing assumptions but all having the common characteristic of predicting an exponential shape for the inclusive cross section. Because these models generally do not have a

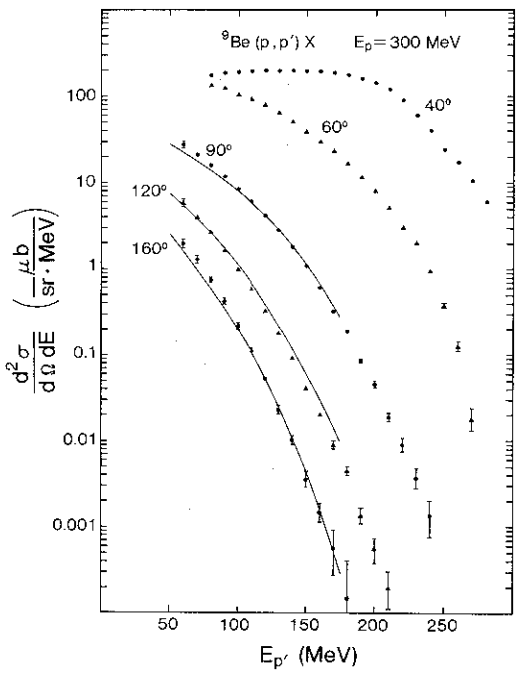

Fig. 1. Single-particle inclusive proton spectra from 300 MeV protons incident on ^{9}Be. The smooth curves for large-angle spectra are described in subsect. 4.3. The statistical errors are shown where they exceed the size of the symbols used.

predictable normalization, it has been difficult to test them on the basis of inclusive data alone, although certainly much progress toward understanding these reactions has been made in the last few years by cross comparisons of the various data sets. Ultimately, however, one has been driven to try more complicated experiments, such as the kind of coincidence experiment described herein, in order to gain further insight into the nature of the reaction mechanism.

Examples of the type of inclusive spectra which one seeks to understand are given in fig. 1 for the ^{9}Be(p, p') reaction at 300 MeV incident proton energy. These data were taken in a measurement subsidiary to the coincidence experiment discussed here in order to provide normalizations for calculations discussed later in this paper; the fits shown for the large-angle spectra are from one of these calculations. While fig. 1 shows, for reference, examples of spectra at more forward angles, our attention here is directed to the study of proton-induced emission of energetic protons at large angles, motivated in part by the hope that such ejectiles may provide information about the short-range NN interaction inside a nucleus [2]).

Two (p, 2p) experiments which have similarities to the one described here have already been reported [4–7]). The common feature of all three experiments is the requirement that one of the protons, which we shall call the trigger, be emitted at a large angle. The important distinction between the past and present experiments

is that a much larger fraction of the kinematic region available to the second proton, which we shall call the forward partner, is measured in the present experiment. This increased fraction is obtained by using a lower incident proton energy of 300 MeV and by using detection systems with modest energy resolution but broad energy acceptance. We have fixed the trigger-proton angle (as did the 800 MeV study), but we have measured with energy differentiation all available trigger energies above 55 MeV as opposed to the three selected values of ref. [4]). Companion protons were measured with energy differentiation for all energies above 65 MeV, as opposed to the more limited samplings in the other studies. In particular, the 640 MeV study [5]) did not include measurements near the kinematic limits for the summed proton energies while the 800 MeV study [4]) concentrated on this region and took only limited samplings outside it. Using a coplanar geometry, we have measured the forward-partner protons from ^{9}Be(p, 2p) reactions at 2° intervals from 14° to 48° and at 4° intervals thereafter to 60° on the opposite side of the beam from 90° trigger protons. This forward-partner angular range extends well above and below the angles leading to minimum residual system recoil momenta. Results from more recent measurements [8]) at $T_p = 800$ MeV encompass a greater range of excitation energies in the residual system than ref. [4]) and display qualitative features in keeping with the results presented here.

Although we will limit our considerations in this paper mainly to the (p, 2p) reaction, it is worth noting that measurements of fragment emission induced by intermediate-energy protons [9–15]) and subsequent efforts to interpret them [16–19]) have made it clear that knowledge of the (p, 2p) reaction for these incident protons is probably a prerequisite for understanding the (p, fragment) data. Moreover, it is important to have information on the (p, 2p) reaction where at least one of the outgoing protons is far removed from the kinematic region accessible in more traditional [20–26]) intermediate-energy quasifree scattering studies which tend to emphasize low residual system recoil momentum and excitation energy.

2. Experimental details

Experimental details of the measurements are given in this section. Two distinct sets of measurements were made but, since many experimental considerations are common to both sets, they are discussed in parallel. One set of measurements was made to determine the ^{9}Be(p, p′) singles spectra of fig. 1. The other set of measurements determined the ^{9}Be(p, 2p) coincidence spectra to be discussed and included one additional ^{9}Be(p, p′) run needed for normalization.

2.1. BEAMS, TARGETS, AND DETECTORS

The incident protons were provided by the TRIUMF accelerator, and the experiment was conducted at the T1 target location on beam line 4B. The intensity of

the incident beam was measured using a polarimeter which was calibrated for this purpose and which was located 3.2 m upstream from the target, and also by a secondary emission monitor (SEM) located 10 m downstream from the target. Typical beam currents on target were 1–20 nA.

The target foils were located at the center of a 0.7 m diameter scattering chamber. For the elastic pp calibration measurements, mylar or CH_2 foils approximately 5 mg/cm^2 thick were used, and were oriented perpendicular to the incident beam. A 48 mg/cm^2 thick Be foil was used for the singles measurements, while a 102 mg/cm^2 thick Be foil was used for the coincidence measurements. The Be targets were oriented at 45° to the incident beam except for a verification measurement made in the region of low recoil momentum quasifree scattering where the target was perpendicular to the beam.

The reaction products were detected by four ΔE-E telescopes which viewed the target through a 0.08 mm thick Kapton window on the scattering chamber. Each telescope consisted of a 76 mm × 76 mm square × 6.35 mm thick NE110 plastic ΔE detector followed by a 102 mm × 102 mm square × 203 mm deep NaI detector. The telescopes were thick enough to stop 280 MeV protons. Each plastic scintillator was viewed via a light pipe by an RCA 8575 photomultiplier tube, and each NaI was viewed by an RCA 2064 photomultiplier tube.

The square face of the plastic detector in each telescope was centered on the square face of the NaI so that a 13 mm wide band was left uncovered around each edge of the NaI. This reduced the position-dependent outscattering contribution to the NaI detector response function so that only one uniform reaction-tail correction was needed.

For the coincidence measurements, one of the telescopes (the trigger) was centered at 90° on one side of the beam. The other three telescopes (the forward partners) were mounted in a coplanar geometry on the opposite side of the beam on a movable boom which could be swung through the angles of interest. The ΔE detector of the trigger telescope was 873 mm from the target and subtended an angle of ±2.5° in both $\Delta\theta$ and $\Delta\phi$. The ΔE detector of each forward partner was 2183 mm from the target and subtended an angle of ±1° in $\Delta\theta$. The forward partners were separated from one another by a scattering angle of 4°.

One run was also taken with the trigger telescope set at a scattering angle of 43° to verify that normal quasifree scattering was observed at low residual system recoil momenta.

The singles measurements were conducted with one telescope whose geometry was identical to that of the forward partners of the coincidence measurement. A telescope was similarly located on the opposite side of the beam for use in calibrating the detectors with pp scattering. During these measurements, a light emitting diode mounted in the NaI housing was periodically pulsed to allow corrections to be made off-line for shifts in gain.

2.2. ELECTRONICS AND ENERGY CALIBRATION

The first requirement for an event of interest in the (p, 2p) measurements was a fast coincidence between the trigger telescope plastic detector and the plastic of one of the forward counters. The resolving time was wide enough to encompass the beam burst from which the trigger event came and the adjacent beam bursts 43 ns to either side of it. If in addition a slow coincidence condition between the trigger NaI and one of the forward counter NaI detectors was satisfied, then a valid event was signalled. All linear signals from the scintillation detectors were then digitized and presented to the computer. The time between the signal in the trigger plastic and the signals from all the other scintillators was also digitized and presented to the computer. All events which were accepted by the computer were stored on magnetic tape for later off-line analysis, and only a cursory examination of the data was performed on-line.

For the (p, p′) measurements, valid events were signalled by a coincidence between the plastic and the NaI (resolving time $\tau \approx 30$ ns). The linear signals from these events were digitized and recorded as in the (p, 2p) measurements.

The energy calibrations for all telescopes were obtained by detecting both protons in the pp elastic scattering reaction. For the (p, 2p) experiment, measurements at five angle pairs gave calibration energies spaced between 66 and 252 MeV for the forward partners and between 48 and 234 MeV for the trigger. For the (p, p′) experiment, seven angle pairs were measured which gave calibration energies between 52 and 240 MeV.

It was necessary to monitor the gains of the NaI detectors because of shifts which occurred as a result of, among other things, variations in the counting rate as the detectors were positioned in the more forward or backward directions. For the (p, 2p) experiments this was made possible by a number of self-consistency checks. In order to achieve stabilization of the gain in the singles measurements an LED was incorporated into the NaI detector for this subsequent experiment. The LED was fired by a pulser at a rate of 5 Hz, and the signals from these events in the NaI detector were digitized and recorded with the (p, p′) events. The signal from a separate output on the pulser was also digitized and recorded as a check of the pulser stability. A bit was set in a coincidence register, whose contents were also recorded for each event, to signal pulser events.

All of the electronics used to process the signals in both measurements were standard commercially available NIM modules. Digitization of the linear signals was performed in standard CAMAC modules which were interfaced either to a Honeywell 316 computer [for the (p, 2p) measurements] or to a PDP 11/34A (for the singles measurements).

Dead-times in both measurements were governed principally by the computer and were determined from the ratios of events accepted by the computer to those

rejected because it was already busy. Dead-times were typically 8–12% for the (p, 2p) measurements and 10–30% for the (p, p′) measurements.

2.3. PROTON IDENTIFICATION

The off-line analysis of the (p, 2p) coincidence data commenced with a check of the TOF information for the plastic detectors. For a given forward-partner telescope, this information was used to tag each event according to whether the forward partner was in prompt coincidence with the trigger (from a reaction or reactions in the same cyclotron beam burst) or in offset coincidence with the trigger (where the trigger event occurred in a reaction from the beam burst immediately following that giving rise to the forward proton) or in neither of these. Within a desired time bin, events involving two protons were easily identified on the basis of the measured energies deposited in each of the plastic and NaI counters. This selection was quite clean; the contribution from deuteron reaction-tail events was very small and there was little interference from pions at the particular energy and angle combinations used.

Proton selection for the (p, p′) singles data was made directly on the basis of a two parameter plot of the plastic amplitude signals versus the NaI amplitude signals. The boundaries of the proton region could not be fixed for all scattering angles because the nature of the background from competing reactions and other sources varied dramatically. At forward angles, events with ΔE values for high-energy protons but with low NaI energy values resulted almost entirely from high-energy protons which did not deposit their full energy in the NaI because they underwent a reaction somewhere in the detector; the contribution from pions to this reaction-tail region was very small as evidenced by the region which contained pion events but no reaction-tail proton events. At large angles, where the proton cross section, especially for high energies, was considerably lower, the relative number of pion events increased dramatically. There was, however, generally a pronounced minimum between the events that were clearly pions and the events that were clearly due to reaction tail effects in detecting the protons. The limits used to define proton events were chosen to be near this minimum. In all cases, conservative estimates of the uncertainties introduced by the procedures used to identify protons have been included in the data of fig. 1.

2.4. RESPONSE FUNCTION CORRECTIONS

Since there is a finite chance that a proton of a given energy will undergo one or more inelastic nuclear reactions when stopping in a NaI crystal, not all protons of a given energy will deposit all of this energy in a NaI detector. To correct the data reported here for the response function of the NaI detectors due to this effect, calculations and data [27]) on the ratio f of events in the reaction tails to events in

the full energy peak were fitted with a functional form

$$f(E) = (E/354)^{1.8}, \tag{1}$$

where E is the full kinetic energy in MeV of the proton. The fit is assumed to be good up to 280 MeV. For our range of proton energies, we expect this fit to be reasonable for protons whose trajectories incident into the NaI are constrained, as in this experiment, to be more than 10 mm from the sides of the crystals [28]).

The forward-partner spectra and the (p, p′) singles spectra were corrected using this fit by starting with the highest energy bin containing data and multiplying the cross section (and statistical error) for this bin by $1.0 + f(E_{max})$, where E_{max} is the midpoint energy of the bin. The cross sections in lower bins were reduced to account for the reaction-tail component that was not included in the E_{max} bin. This reduction, including the appropriate addition in quadrature of the statistical errors, used two different algorithms. For the earlier (p, 2p) analysis, the reaction-tail contribution to the lower energies was simply assumed to be uniform from a proton energy of zero to the lowest energy in the E_{max} bin. For the later (p, p′) runs, an investigation of the pp elastic scattering runs indicated that a better fit to this reaction-tail component was obtained by assuming it increased linearly from zero at zero proton energy to a maximum at the lowest energy in the E_{max} bin and so we used this assumption for correcting the (p, p′) inclusive spectra. The quality of such a fit is

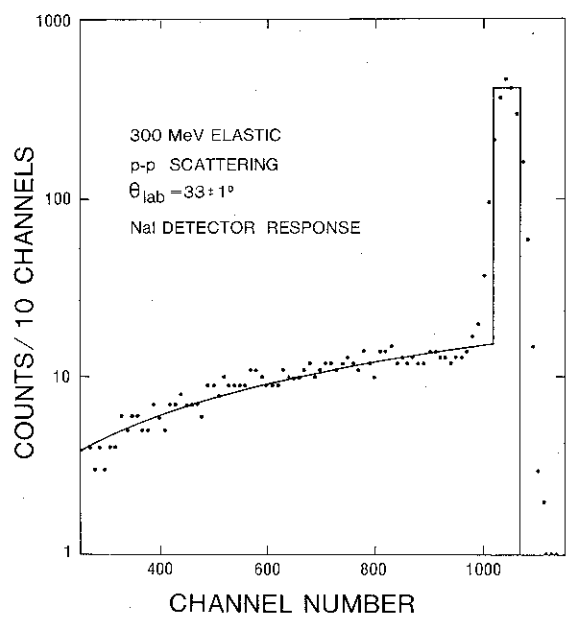

Fig. 2. The response of the NaI detector systems to elastically scattered protons between laboratory angles of 32° and 34° from 300 MeV protons incident on ^1H. The solid curve, normalized to the same overall area as the data, is the response which would be assumed by the inclusive spectra correction algorithm described in the text.

indicated in fig. 2 where the spectrum resulting from elastic pp scattering yielding protons of approximately 200 ± 5 MeV is shown along with a fit to the data using the latter algorithm. The width in the fit to the peak is the expected kinematic width due to the angular acceptance of the detectors and the area under the fit has been set equal to that expected from the total number of counts observed. For the (p, 2p) runs, no reanalysis was undertaken because tests to see if the data should be corrected using the newer algorithm indicated differences in the final results were smaller than the statistical errors in the data.

After correcting the highest energy bin in a spectrum as just described, the same procedure was used repeatedly on sequentially lower energy bins with appropriate $f(E)$ values until the entire spectrum had been corrected. The propagation of the statistical errors by the procedure is appropriately reflected in the final values which result.

No response function corrections were included for the trigger telescope because the normalization used for the (p, 2p) data automatically corrected for the $1+f$ factor and the steeply falling (p, p′) inclusive cross section at 90° as the scattered proton energy increases meant that effects from the reaction-tail subtractions were negligible.

3. Results

3.1. UNITS, DISPLAY VARIABLES, AND ACCURACIES

Since the main purpose of this investigation was the study of energetic proton emission at large angles, the (p, 2p) data are presented in terms of the numbers of forward-going protons of given energy (E_f) and direction (θ_f and ϕ_f) associated with large-angle trigger protons of given characteristics (E_q, θ_q, and ϕ_q). We present our (p, 2p) results in terms of the associated proton double differential mean multiplicity

$$\frac{d^2\langle m\rangle}{dE_f\, d\Omega_f} = \frac{d^4\sigma(E_q, \theta_q, \phi_q; E_f, \theta_f, \phi_f)/dE_q\, d\Omega_q\, dE_f\, d\Omega_f}{d^2\sigma(E_q, \theta_q, \phi_q)/dE_q\, d\Omega_q}, \tag{2}$$

where the trigger particle q is here a proton (we intend in future to study this quantity for cases where the trigger particle q will be other selected fragments). The name we have chosen for this quantity stems from the relation

$$\int_{4\pi} d\Omega_f \int_0^{max} dE_f \frac{d^2\langle m\rangle}{dE_f\, d\Omega_f} = \langle m(E_q, \theta_q)\rangle \tag{3}$$

which is the total associated mean proton multiplicity for fragments q (protons here) at θ_q and E_q. Using $d^4\sigma/dE_q\, d\Omega_q\, dE_f\, d\Omega_f$ directly, as does ref. [5]), is perfectly acceptable but this quantity has a rapidly varying dependence on E_q of the large-angle trigger and we find the data more convenient to display and interpret if we

remove this by using mean multiplicities. Part of the systematic uncertainties in normalization are also removed from our data by using mean multiplicities because we use (p, p′) values for $d^2\sigma/dE_q\, d\Omega_q$ measured with the trigger telescope during the (p, 2p) runs, thus ensuring identical geometries and electronic settings for the trigger telescope contributions to both cross sections in eq. (2). The form used in ref. [4]) to present their data is similar to ours except that it retains factors dependent on their particular geometry.

To increase the statistical accuracy of the display points, it is necessary to use finite energy bins of significant magnitudes. This introduces an artificial additional width to most sharp energy dependences if one works directly with E_f and E_q as independent variables in the differential multiplicity. To retain as well as possible the most likely sharp energy dependence, we use E_q and $E_{sum} = E_q + E_f$ as the independent variables in energy for differential multiplicities and can thus retain good definition in residual system excitation energy. This is done by adding E_q and E_f at the individual event level before subsequent binning operations. Excitation energy dependences are then displayed to a level determined almost solely by the accuracies attainable in the NaI detectors. The observed spreading about the expected kinematic region in fig. 2 gives an idea of the resolution of the NaI detectors. We estimate the experimental width in measured excitation energies in this work is of order ±5 MeV but that the absolute precision is limited to ±10 MeV at large $E_f + E_q$ because of uncertainties in the gains of the NaI systems. This precision is quite adequate to demonstrate a number of significant features in large-angle-triggered (p, 2p) processes.

The relative accuracy in the magnitudes of the mean multiplicity values for different forward-partner angles is determined predominantly by how well the companion singles measurement in the trigger telescope can be normalized to the (p, 2p) runs. Two sources of error are important in this regard for the present experiment. First is the relative accuracy of the beam monitors. The two independent beam monitors used agreed in relative value with a 2% standard deviation in the ratio of the values. Second is the uncertainty in relative normalization from incorrect assignment of trigger proton energy due to gain shifts. The magnitude of this effect depends somewhat on the energy of the trigger proton but we estimate that it should not exceed ±5% for the majority of our data. The final results, assuming one can expect relatively smooth changes in the 2° steps, indicate generally better agreement than this. Other sources of error in relative values of the multiplicity at different angles, such as changes in location of the beam spot on the target coupled with target nonuniformity, are estimated to be small (≤2%).

In addition to the same sources which contribute to errors in the relative values between angles, the absolute values of the mean differential multiplicities are subject to uncertainties from errors in the forward-partner solid angles Ω_f and from the accuracy of the NaI response function correction (this latter source also contributes to a lesser extent to uncertainty in relative values for different forward energies

E_f). We estimate this overall accuracy in mean multiplicity values as ±10%. Neither this error nor the relative angular error are included in the figures presented since they are frequently unimportant to the conclusions to be drawn.

Uncertainties in the normalizations of the ^{9}Be(p, p′) inclusive proton spectra are dominated by those in the absolute calibration of the beam monitors, in the NaI response function, in the angular setting of the target, and in the solid angle of the telescope (mainly from edge effects due to outscattering at high proton energies). Most of these have been considered in some detail by previous experiments using NaI detectors in the same target area [24–28]). We estimate the combined uncertainty in these inclusive spectra normalizations to be ±5% relative and ±15% absolute except at 160° where there is an additional ±10% error because of interference with the proton identification from a significant background of diffuse events.

3.2. REAL VERSUS ACCIDENTAL EVENTS

As mentioned earlier, the resolving time of the coincidence between a forward counter and the trigger counter was large enough to encompass coincidences between events from the same beam burst and the bursts before and after. This enables information to be acquired at the same time on both real and accidental coincidences. Shown in fig. 3 are the summed energy spectra for the prompt time bin (real plus accidental events), the spectra for an offset time bin (accidentals only) and the difference between these (real events, but which have not yet been corrected for the NaI response function) for four forward angles triggered by protons at 90° with energies between 75 and 85 MeV. At the larger forward angles measured, the accidentals spectra reflect essentially just the untriggered singles spectra multiplied by a number depending on the product of the singles rates in the forward and trigger telescopes. At the smaller forward angles, this relation no longer holds because the range of kinematically allowed ^{9}Be(p, p′) scattered protons can exceed the total telescope thickness. Thus the measured accidentals spectra have components which result from the folding back of higher-energy components of the actual singles spectra. This makes it difficult to extract the precise singles spectra at angles less than approximately 30° but it is clear that the back folding at smaller angles would not obscure the sharp structure seen in the coincidence spectra if the latter existed to the same extent in the singles spectra.

The foldback problem in the small-angle singles spectra makes a quantitative comparison of the shapes of singles angular distributions and coincidence angular distributions difficult. However, it is clear that for most forward-energy values selected for such a comparison, the singles distributions generally have much different variation than the coincidence distributions to be discussed here. This is certainly true of energy-integrated angular distributions (above forward energies of approximately 70 MeV) where the folded spectra can be treated well enough to see that the singles angular distributions decrease monotonically while, for every

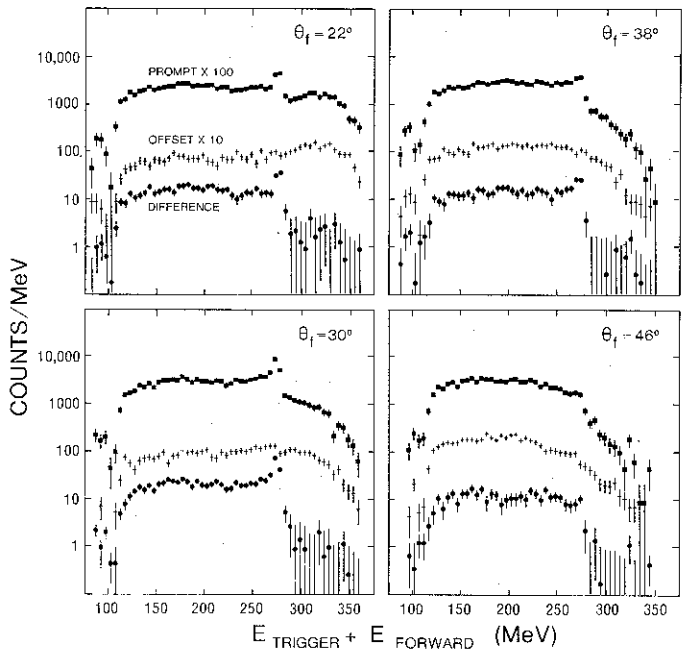

Fig. 3. Raw summed energy spectra (no corrections for detector response) from ^{9}Be(p, 2p)X reactions at $E_p = 300$ MeV for 90° trigger energies between 75 and 85 MeV for various forward proton angles θ_f. Shown are spectra for forward events in prompt coincidence with the trigger (■, reals plus accidentals), in offset coincidence with the trigger (+, accidentals only), and the difference (●, real events).

large-angle trigger energy measured, the energy-integrated coincidence spectra peak at some forward angle in the measured range, as shown in fig. 4.

This situation can be contrasted with data [4]) obtained for 800 MeV protons incident on ^{6}Li. In that case, the angular distributions of forward protons in three selected energy bins (corresponding to three different trigger proton energy bins) showed that the only difference between the singles and coincident forward proton cross sections was the overall magnitude, i.e. the shapes of the angular distributions were identical. This was an unexpected feature for these data, and has been used [6]) as a crucial piece of evidence against models which originally motivated these measurements. Our measurements at 300 MeV do not indicate such a relationship between singles and coincidence spectra.

3.3. GENERAL FEATURES OF MEAN MULTIPLICITY DISTRIBUTIONS WITH SUMMED ENERGY

Figs. 5 and 6 show some of the measured differential mean multiplicities as a function of the summed proton energy. Fig. 5 displays $d^2\langle m\rangle/d\Omega_f\, dE_f$ at $\theta_f = 30°$

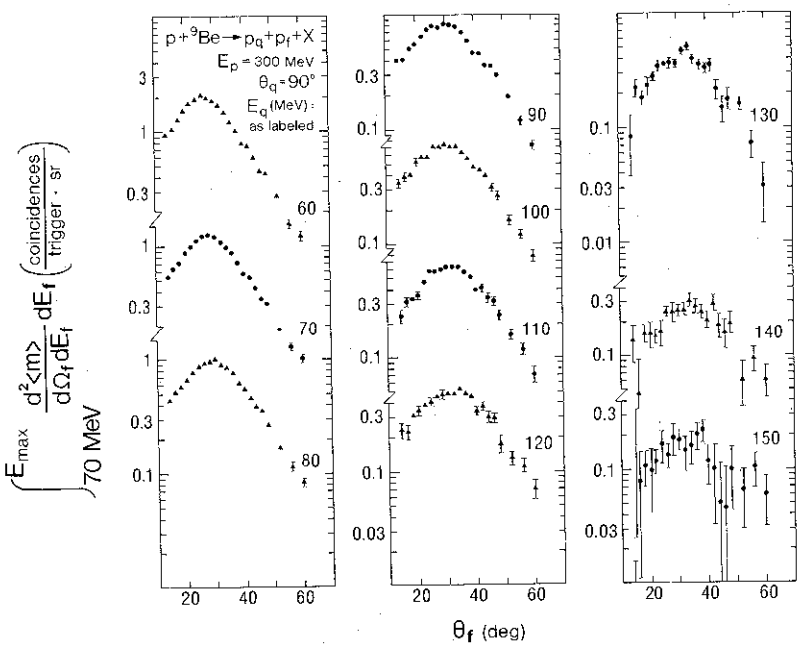

Fig. 4. The integral over forward-proton energies above 70 MeV of the measured differential mean multiplicities as a function of forward-proton angle for various trigger-proton energies. Statistical errors are indicated where they significantly exceed the symbol size.

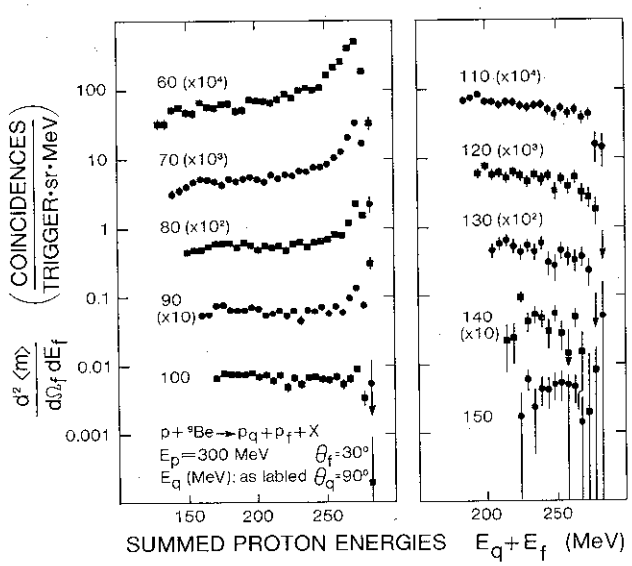

Fig. 5. Differential mean multiplicities as a function of the summed energies of the two outgoing protons. Spectra are shown for trigger protons of various energies E_q emitted at 90° on one side of the beam and forward protons emitted at 30° on the other side. Errors shown are statistical only.

for various trigger proton energies E_q. Ten MeV wide bins centered on the stated values have been used for the trigger protons. Fig. 6 displays $d^2\langle m\rangle/d\Omega_f\, dE_f$ for $E_q = 70 \pm 5$ MeV for various forward partner angles θ_f. Bins for the summed energy $E_f + E_q$ are 5 MeV wide.

At values of $E_f + E_q$ below the kinematic limit by more than approximately 25 MeV, the distributions in figs. 5 and 6, as well as the other such distributions measured, are slowly varying as a function of $E_f + E_q$, at least within the available statistics. Near the kinematic limit, some of the distributions show a significant increase in value above the roughly uniform values below the kinematic limits. The enhancement above the uniform value decreases as the trigger proton energy increases or as the forward-partner angle is moved significantly away from the angle yielding minimum values of the recoil momentum k in the undetected residual system. Enhancement above the uniform level is limited to cases where it is possible to have $k \lesssim 300$ MeV/c and the enhanced region is probably best analyzed by conventional calculations of proton knockout from $p_{3/2}$ shell-model states using the DWIA formalism. It is not the intent in this work to investigate this type of process for which much more appropriate studies already exist [20–26]), except to the extent that it represents one of the contributions to large-angle inclusive spectra.

While the peak in the near-coherent-recoil region is certainly the most dramatic feature in those summed energy distributions where it occurs, it does not represent

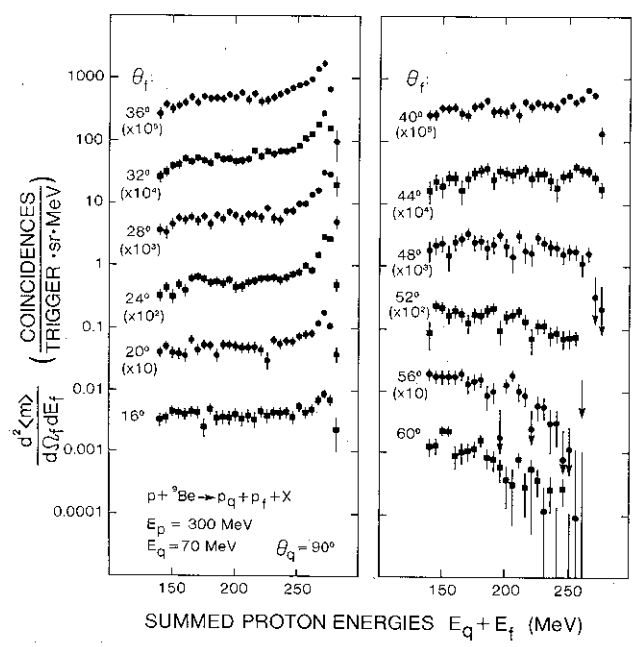

Fig. 6. As in fig. 5 except spectra are shown for a fixed trigger-proton energy of 70 ± 5 MeV for various coplanar opposite side forward proton angles θ_f.

the major share of the forward-proton multiplicity associated with the 90° trigger protons we observe. The rather featureless continuum in forward proton energy must therefore be one of the results predicted by any model purporting to explain large-angle proton emission accompanied by emission of other protons.

3.4. SUMMARIZED EXPERIMENTAL RESULTS

A concise presentation of the mean multiplicity data is allowed by the features of the energy distributions discussed in the last subsection. Since the only observed rapid variation with summed proton energy E_f+E_q occurs near the kinematic limit, the overall nature of the data can be displayed by giving the forward-partner angular distributions of the average value of the associated differential multiplicity for a few representative regions in summed energy. A region encompassing the uppermost 25 MeV kinematically allowed for E_f+E_q displays the behavior of these large-angle-triggered (p, 2p) processes when the residual system recoils coherently or near coherently with little or no excitation energy. Angular distributions for this region are shown in fig. 7.

At energies below this approximately coherent-recoil region, the variation with E_q+E_f is sufficiently slow that the data can be averaged over even larger regions

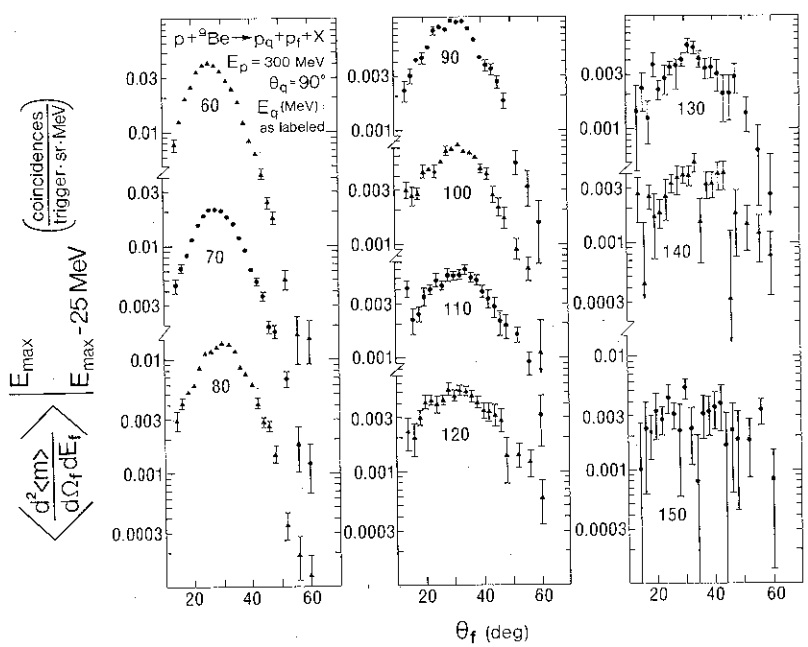

Fig. 7. The average values of the differential mean multiplicities over a selected summed energy interval as a function of the forward-proton angle for various trigger-proton energies. Statistical errors are shown where they significantly exceed the symbol size. The energy interval selected for this figure is the uppermost 25 MeV kinematically allowed.

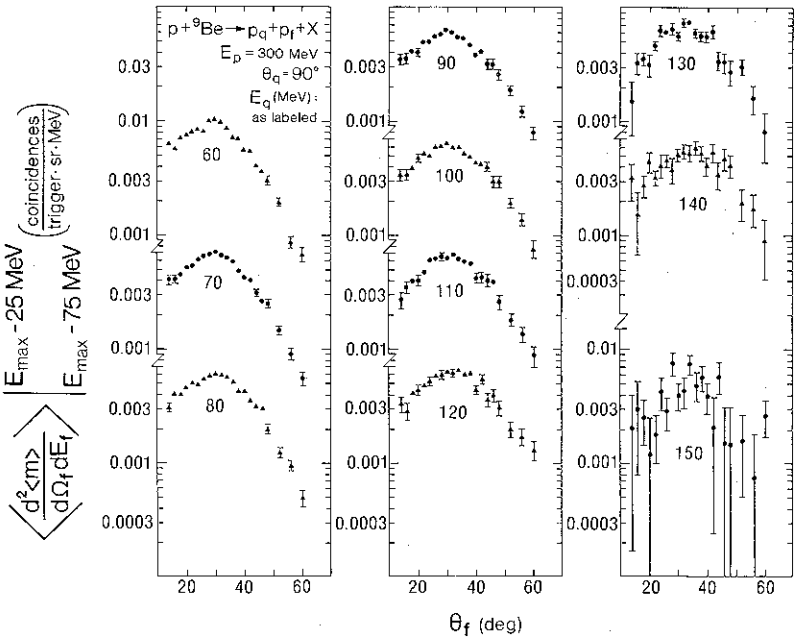

Fig. 8. As in fig. 7 except the summed energy interval selected is the 50 MeV (or as much of it as was measured) below an energy 25 MeV less than the kinematic limit.

without significantly obscuring the level of detail available in the data. Fig. 8 shows results for the 50 MeV region (or as much of it as is available in the data) immediately below the region in E_q+E_f shown in fig. 7. Fig. 9 shows the results for the region in E_q+E_f immediately below that for fig. 8. For fig. 9, the average is taken over the remainder of the measured energy range below the two regions of figs. 7 and 8.

Several interesting features of the data can be seen in figs. 4 and 7 through 9, in particular the contrast between the near-coherent-recoil (CR) region and the remainder of the data. At the lower trigger energies, the angular dependence of the CR data is more sharply peaked than that of the remaining data and the magnitudes at the peak angles are much higher than those of the other regions. As the trigger energy is increased, these differences become less pronounced and eventually the magnitudes of the CR data fall below those of the lower summed energy data. The magnitudes of the maxima for the CR region data in fig. 7 change by a factor of approximately ten as the trigger energy is changed from 60 to 150 MeV while the corresponding magnitudes in fig. 8 change only by a factor near two. The change over the range of trigger energies available in the data of fig. 9 is even less.

The angular values θ_M at which the various distributions in figs. 4, 7, 8 and 9 peak are of considerable interest in terms of some of the models to be discussed

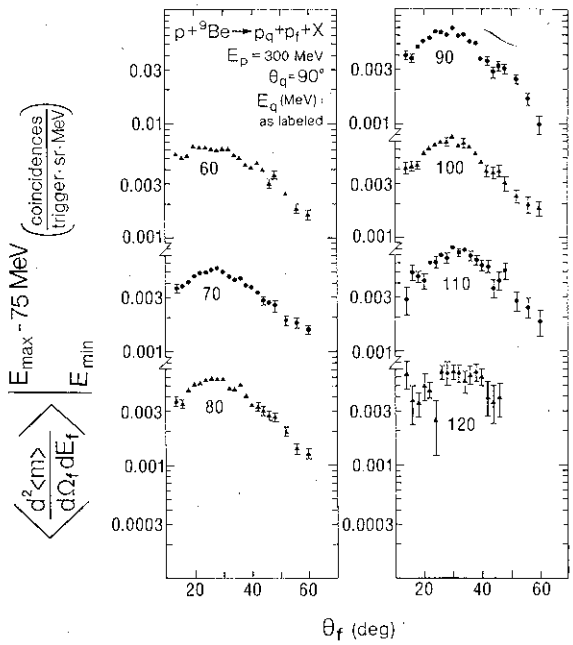

Fig. 9. As in fig. 7 except the summed energy interval selected is all measured energies below 75 MeV less than the kinematic limit.

in sect. 4. Where the statistical accuracy of the data is sufficient, we have extracted values for these θ_M's with an estimate of our precision by fitting the distributions in these figures with a gaussian shape on top of a quadratic background, both centered at the same angle. Fig. 10 shows some of the results as well as the angles, often called QTBS angles, corresponding to minimum residual system recoil momentum for trigger angles of 87.5° and 92.5° (spanning the angular range of the trigger in this experiment). Error bars on the angles θ_M indicate the accuracy to which the parameter is determined assuming the five-parameter functional form used is correct. At low trigger energies, the θ_M's for different regions in summed proton energy clearly differ from each other and from the QTBS angles. As the trigger energy increases, these differences in θ_M's appear to decrease (except perhaps for the rapidly diminishing highest-summed-energy component). The statistical accuracy of the data prevents firm conclusions at the highest trigger energies.

A convenient way to visualize the data for a given trigger energy and angle is provided by contour plots of $d^2\langle m\rangle/d\Omega_f\, dE_f$ on a polar grid in θ_f and E_f. This gives a global view at the expense of detail. Examples for trigger energies of $E_q = 70$ and 110 MeV are given in figs. 11 and 12. Included in the figures are indications of the kinematic and instrumental limits of the measurements.

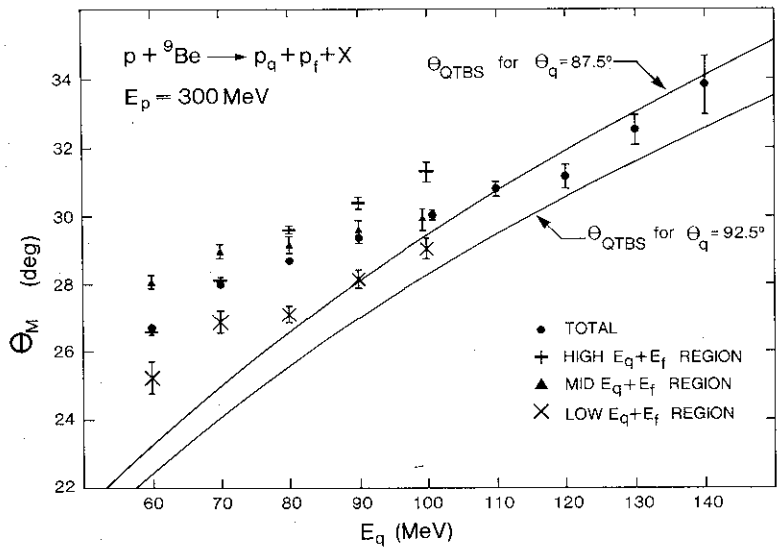

Fig. 10. Forward-partner angles θ_M corresponding to maximal differential mean multiplicities for various regions in summed proton energy (corresponding to figs. 4, 7, 8 and 9). Angles for minimum residual system recoil momenta (QTBS angles) are shown for the two extreme angles subtended by our trigger telescope. Errors shown are from the fit described in the text and reflect only the accuracy with which the five-parameter symmetric distribution assumed can be used to extract the θ_M's.

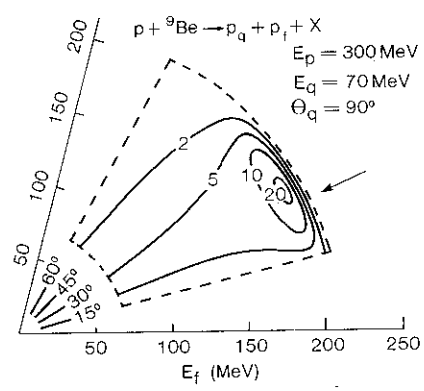

Fig. 11. Contours of constant mean differential multiplicity (in units of coincident protons/MeV · sr · 1000 trigger protons) associated with fixed-energy coplanar trigger protons observed at 90° on the opposite side of the beam. The contours are shown on a polar grid in energy and emission angle of the coincident proton. The dashed outline is either the limits of the experimental measurements or the kinematic limit. The arrow indicates the QTBS angle associated with the trigger-proton energy of $E_q = 70$ MeV.

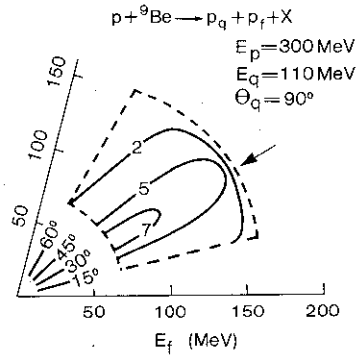

Fig. 12. As in fig. 11 except for a trigger-proton energy of $E_q = 110$ MeV.

The arrows in figs. 11 and 12 show the forward-partner QTBS angles for the nominal trigger energy proton at the nominal opposite side 90° scattering angle. From these figures and fig. 10, one can see that the coincidence rates, at least for low E_q, generally peak at slightly larger angles than the QTBS angles as was also found for the ^{6}Li(p, 2p) measurements at 800 MeV [ref. [4]]. At our higher trigger energies, the data appear to approach the QTBS angles. The significance of features in these plots will be discussed later in light of various models of the (p, 2p) reaction.

The data in fig. 4 can be integrated over angle to give an idea of the contribution of multiple energetic proton emission to large-angle inclusive proton spectra. Table 1 shows results for two such integrals for various trigger energies. The first integral represents the overall multiplicity actually observed in the very restricted out-of-plane region subtended by our forward detectors. The second integral represents an estimate of associated multiplicity of forward protons above 70 MeV and is

TABLE 1

Mean multiplicities measured in the solid angle subtended by the experiment and overall mean multiplicities calculated from the data

E_q (MeV)	~% of E_f range measured	$\langle m\rangle_{meas} = \sum_{\text{measured values}} \Omega_f \frac{d\langle m\rangle}{d\Omega_f}$	$\langle m\rangle_{calc}$ for $E_f > 70$ MeV
60	68	0.028	0.50
70	67	0.018	0.32
80	65	0.015	0.26
90	63	0.013	0.22
100	61	0.012	0.22
110	59	0.010	0.18
120	56	0.0086	0.15
130	53	0.0068	0.11
140	50	0.0047	0.09
150	46	0.0029	0.05

obtained by assuming the out-of-plane dependence is such that the differential multiplicity is symmetric around an axis passing through the in-plane angle at which the differential multiplicity is maximal. This symmetry is consistent with our in-plane data, except perhaps at $E_q = 60$ MeV. Values obtained from the average of the in-plane angles symmetric about the maximal axis are used for the integration where data on both sides of the axis exist. Beyond that point, the single available value is used, and the integral is terminated at the outermost data point measured. Also shown in the table are the approximate percentages of the available forward-proton energy ranges (which are not identical to the available forward-proton phase space) which are measured in this experiment (for a given trigger energy these of course vary slightly with forward angle).

The associated multiplicities in table 1 for the higher trigger energies fall off much more rapidly than would alone be suggested by the fraction of the forward energy range measured. However, figs. 7 through 9 indicate an increased weighting toward lower allowed forward proton energies as the trigger energy increases and the decreased multiplicities may in part be due simply to the fact that the associated protons were below our measured energy range. The angular distributions of fig. 4 are also less sharply peaked at higher trigger energies and, coupled with the weighting factor involved in the angularly symmetric integration, this will lead to including a lesser fraction of the coincident protons inside the measured angles at which we have terminated the integrals. The overall multiplicity associated with trigger protons at 90° will be determined predominantly by the lower trigger proton energies because they are much more numerous. In general, we find forward protons to be associated with large-angle protons a significant fraction of the time, in contrast to the results [4]) for 800 MeV incident protons where only a limited range of forward energies was considered.

3.5. COMPARISON WITH FORWARD-ANGLE-TRIGGERED DATA

It is of some interest to contrast the large-angle results with the kinematic regime of more conventional (p, 2p) measurements. While this experiment was not optimized to do so, some estimates of forward-triggered associated multiplicities can be made by using our ^{9}Be(p, p′) data at 40° to normalize the 43° triggered (p, 2p) data taken to verify system performance during the coincidence measurements. Unfolding the NaI detector response function corrections for the continuum regions in the forward-triggered (p, 2p) data is considerably more complicated than at back angles where one can effectively neglect the contributions to lower trigger energies from higher trigger energies. We have not attempted to correct the forward (p, 2p) data for response function and have used instead this uncorrected data normalized by the 40° singles data, also not corrected for response function, to generate response-function-modified multiplicities such as those of fig. 13. One should also note that aside from this response function problem and the difference between

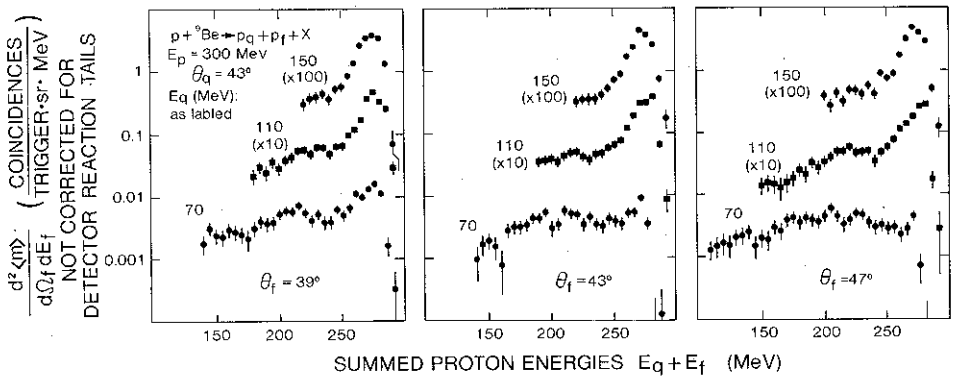

Fig. 13. Detector response modified differential mean multiplicities for 43° proton triggered ^{9}Be(p, 2p)X reactions at $E_p = 300$ MeV as a function of the summed energies of the two outgoing protons. Spectra are shown for coplanar coincident protons emitted at 39°, 43° and 47° on the opposite side of the beam from the trigger proton for three selected trigger-proton energies. Errors shown are statistical only; see text for a discussion of other sources of error. The lower energy cutoffs in the $\theta_f = 47°$ detector system were lower than in the other systems and the data points shown for this case have been correspondingly extended downward in energy.

40° and 43°, the singles spectrum used in this case is taken with different detector geometry and electronic settings than those of the trigger telescope thus losing the benefits of some of the error cancellation found in the majority of our data.

In spite of the reservations associated with the forward-triggered data, sufficient accuracy exists that interesting comparisons can be made using it. While the cross sections are significantly larger at forward angles, the associated double differential multiplicities are often smaller than at larger trigger angles, especially for data in the continuum regions. This is most likely due to the larger angular region available to the forward proton for a given limit on the residual system recoil momentum.

One also sees in the forward-triggered data a behavior for the near-coherent-recoil region similar to that seen in the large-angle-triggered data, with one slight and understandable difference. Where the energies and angles of the two observed protons are such that a large residual system recoil momentum k is required (e.g. low trigger energies E_q in fig. 13, large θ_f in fig. 6, or large E_q in fig. 5), the coherent-recoil region is suppressed relative to the continuum region. As k is decreased somewhat in either trigger geometry, a narrow structure appears near the kinematic limits of the spectra. As k decreases to values lower than those possible in the large-angle data (nearing zero for 150 MeV triggers in fig. 13), the peak region broadens somewhat in width. This is probably due to an increased contribution from $s_{1/2}$ proton knockout as k nears zero.

4. Theoretical analysis and interpretation

4.1. GENERAL COMMENTS ON INCLUSIVE SPECTRA AND THEIR RELATION TO THE MEASURED COINCIDENCE SPECTRA

At first glance, the fact that so many of the inclusive spectra for various projectile-target-ejectile combinations are approximately exponential with ejectile energy might give one hope that there is a universal reaction mechanism operating and that one can assume that what is learned from one particular projectile applies equally to all others. However, intuition tells us this is not likely to be true, and experiment seems to be confirming this. For example, in a heavy-ion collision, projectile nucleons have a significant chance of undergoing many NN collisions, both with target nucleons and other projectile nucleons, in traversing the interaction region. After a few times 10^{-22} sec, it may then be appropriate to describe part of the interaction region as a system of nucleons which, in some reference frame, has a thermal distribution of energies. At the other extreme, the likelihood of forming such a thermalized hadronic system in electron or muon induced reactions is greatly reduced, owing to the facts that the projectile is not a composite object and that it undergoes, at best, only a few collisions because of the weakness of the coupling constant involved. Hence, lepton-induced reactions are more likely to have a strong direct component, while heavy-ion reactions are more likely to have a strong statistical component. For inclusive spectra from proton-induced reactions, the relative importance of each of the many possible reaction mechanisms probably lies between that for heavy-ion reactions and that for leptons or photons. While protons interact strongly with target nucleons, the number of NN collisions per unit volume will be lower than that attained with composite projectiles.

By selecting certain portions of inclusive spectra, one can hope to emphasize kinematic regimes where only one type of reaction mechanism is dominant. A graphic example of such a region for (p, p′) spectra from 800 MeV incident protons is provided by the quasielastic peak seen in the forward-angle inclusive spectra of ref. [29]). Unfortunately, for the majority of inclusive spectra which show only a nondescript exponential behavior, such regions are more difficult to define. Much recent work has focussed on energetic ejectiles at large angles often in the hope that kinematic constraints resulting from this combination would emphasize reaction mechanisms involving a minimal number of NN interactions [15–19,30–40]). Whether such a hope is fulfilled can, it appears, only be assessed by performing measurements yielding more details about the interaction than do the single-particle inclusive spectra by themselves [41]). If indeed regions can be found which minimize the number of NN interactions, it may be possible to relate inclusive spectra from various sources in a manner which is more informative than at present.

The incident energy at which we have chosen to work is somewhat lower than in most related studies, but the reaction mechanisms responsible for the inclusive

spectra should not differ greatly. The inclusive (p, p′) cross sections which we measured at 300 MeV incident kinetic energy are displayed in fig. 1. The behavior of these spectra at large angles is similar to that observed at 500 and 800 MeV, namely a roughly exponential decrease in the cross section as a function of ejectile energy, becoming steeper with increasing angle. The origin of the smooth curves through the data will be described shortly, but it is worthwhile pointing out here that they were generated by a model [17]) which was developed to describe the (p, p′) reaction at higher energies. Only small changes in the parameters determined at 800 MeV were made to fit the data at 300 MeV. This gives us some confidence that there is nothing particularly novel or unusual about the relatively low projectile energy which we have chosen, and that the conclusions which we draw from our coincidence measurements should have some general significance.

The exact choice of target for the experiments reported here was not considered critical. It has been pointed out [42]) that, at fixed ejectile energy and angle, the (p, p′) inclusive cross section per target nucleon is roughly constant as a function of target mass number A_T for targets [43]) from ^{4}He to Ta although it does increase slowly for heavy targets. This suggests that the same reaction mechanisms may apply for most target masses, although multiple scattering processes must be more important for heavy targets. If there is a direct component, any correlation between the two observed protons in (p, 2p) measurements may be washed out in a heavy target. Since we are particularly interested in evaluating direct components of the (p, p′) reaction, a convenient light target, namely ^{9}Be, was chosen for these studies.

In the remaining portions of this section, several models for reactions leading to inclusive particle production are discussed in light of previously existing measurements of various types and in light of the current ^{9}Be(p, 2p) data.

4.2. THERMAL AND PHASE-SPACE MODELS

There is already evidence that energetic wide-angle particle emission is not predominantly statistical in origin. The evidence from inclusive reactions is, firstly, the approximately constant value of the (p, p′) cross section per target nucleon from ^{4}He to Ta at 90° emission angle [43]). It is difficult to imagine how four of five nucleon systems, such as are involved in the ^{4}He experiment, can behave statistically. The constancy of $(1/A_T)\, d^2\sigma/d\Omega\, dE$ as a function of A_T implies this conclusion is probably at least partially valid for heavier targets as well. The second piece of information is the value of about 2 obtained [44]) for the (p, p′)/(p, n) ratio at 100 MeV incident proton kinetic energy. This ratio is expected [45]) to be about two in a direct knockout model, and roughly unity in an evaporative model.

Assuming common reaction mechanisms as a function of A_T, one can also extrapolate conclusions from heavier targets to lighter systems. If one hypothesizes that energetic ejectiles arise from emission from a thermally equilibrated source, then one can use the exponential slope of the differential cross section as a measure

of the temperature of the source. In such an analysis, the temperatures turn out to be in the tens of MeV range [1]), in contrast to the few MeV range found for the low-energy evaporative peak. These high temperatures are seen even for 200 to 500 MeV incident protons on Ag and could not be reached if the entire nucleus as a whole were acting as a source: if one spreads the incident proton's kinetic energy over a hundred or so nucleons then, in the intermediate-energy range, a temperature in the few MeV range will result. Hence, the "thermal" source would have to be much smaller than the medium-mass target itself, say of order 10 nucleons [46]).

This small value for the number of nucleons in the thermal source even for massive targets can also be found by other means. Again, the kind of analysis which gives one the source's temperature also gives one its velocity. Assuming for intermediate-energy protons incident on Ag that the incident proton's entire momentum goes into the source, then the number of nucleons in the source can be shown to be in the 10 nucleon range. If the incident nucleon loses only a fraction of its momentum, the source must be even smaller. This thermal model analysis consistently points towards a small, hot source. While it might be possible to conceive of a ^{9}Be target leading to such an unlikely source, the results of the present (p, 2p) measurements limit this possibility.

One would expect that a thermal model would not predict the kind of leading-particle effect shown in figs. 11 and 12. If the trigger proton arises from a hot spot with a temperature of the order of tens of MeV and with tens of MeV in translational energy, then the incident proton has presumably lost most of its energy to the hot zone. Hence, one would expect that the protons observed in coincidence with the trigger would possess the usual exponential thermal spectrum, perhaps of lower average temperature if the source comes to a new thermal equilibrium after emission of the energetic trigger particle. On the basis of the (p, 2p) experiment presented here, one cannot rule out such a hot-spot contribution to the inclusive spectrum in that this experiment did not measure forward protons with energy down into the 20–70 MeV range. Nevertheless, because such a substantial fraction of the inclusive events are accompanied by a leading particle strongly correlated in angle with the trigger, at best the hot-spot model will be only one contributor among several in this incident energy range.

One can draw a similar negative conclusion about statistical models in which the phase space available to the recoiling objects is evaluated explicitly [47]). The following, rather simple, calculation will suffice to show how this conclusion is reached:

Assuming that a sufficient number (N) of nucleons are recoiling from the trigger and forward protons that they can be assumed to be non-relativistic, then the integral over their associated phase space,

$$R_N \equiv \int \prod_{i=1}^{N} \frac{d^3 p_i}{2W_i} \delta^4\left(K - \sum_i p_i\right), \tag{4}$$

where K is the overall four momentum of the N particles, is given by [48])

$$R_N = \frac{(2\pi^3)^{(N-1)/2}(\prod_{i=1}^{N} m_i)^{1/2}}{2\Gamma[3(N-1)/2](\sum_{i=1}^{N} m_i)^{3/2}}\left(\mathcal{M}_k - \sum_{i=1}^{N} m_i\right)^{(3N-5)/2}, \tag{5}$$

where $\mathcal{M}_k$ is the invariant mass of the N-particle system of total energy W_k and momentum $\boldsymbol{k}$. Let us assume that these N recoiling objects are all nucleons, so that eq. (5) simplifies to

$$R_N = \frac{(2\pi^3)^{(N-1)/2}}{2N^{3/2}\Gamma[3(N-1)/2]} m^{(N-3)/2}(\mathcal{M}_k - Nm)^{(3N-5)/2}. \tag{6}$$

This expression cannot reproduce the strong enhancement observed at near-coherent residual system recoil for trigger protons in the 70 MeV range. Is it, however, a reasonable description of the continuum region? Again, the expression cannot reproduce the dependence of the differential mean multiplicity as a function of forward-proton energy, as exemplified by figs. 5 and 6. The term $\mathcal{M}_k - Nm$ in eq. (6) increases rapidly as the forward proton momentum p_f decreases from its maximum value. Because this term is raised to a power, R_N increases very rapidly as p_f decreases. Indeed R_N may increase by several orders of magnitude over the range of p_f measured here (at fixed θ_f) whereas the data are roughly constant.

Even if the kinematics are arranged so as to minimize the variation of $\mathcal{M}_k - Nm$, by fixing $|\boldsymbol{p}_f|$ but varying θ_f, this phase-space model does not reproduce the angular dependence. An example is shown in fig. 14, where a comparison is made with the averaged differential multiplicities of fig. 8. The forward-proton energies were fixed at 170 and 130 MeV for trigger-proton energies of 70 and 110 MeV. These energies represented (roughly) the average of the forward energies in the data (since the data are roughly constant over this energy range, the choice of forward energy is not crucial). Of course, the normalization of this model is not determined, and so we have fixed it by normalizing to the data at 20°. Clearly then, the energy dependence of the data is not reproduced by this model and even the angular dependence of the model lacks the ability to reproduce the sharpness in peaking near the QTBS angle observed in the data.

4.3. DIRECT KNOCKOUT MODELS

Models at the other extreme from the thermal and phase-space models are the direct knockout models, in which the projectile undergoes a single collision with an off-shell nucleon in the nucleus, the latter then becoming the observed ejectile (at least for wide angle scattering). The NN collision is then a low 4-momentum transfer process, much of the ejectile's momentum originating from its off-shell nature in the nucleus before the collision. Such an off-shell nucleon presumably arises from short-range NN interactions. Many-body calculations of these high momentum components of the single-particle nuclear wave function do show a

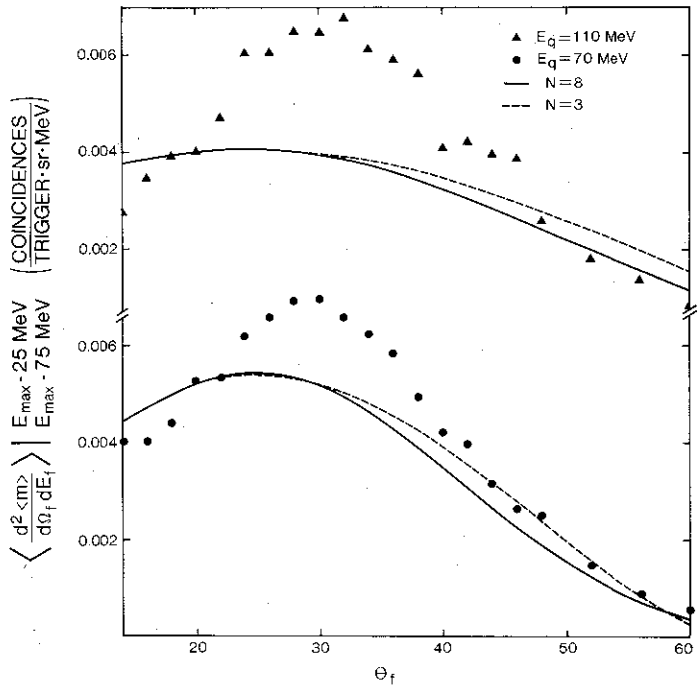

Fig. 14. Comparison of non-relativistic phase space for N recoiling nucleons for examples of the data shown in fig. 8. The trigger energies chosen are 70 MeV (circles) and 110 MeV (triangles). In both examples, the theoretical curves were normalized to the data at 20°. See text for a discussion of the failure of this model to predict the observed outgoing proton energy dependence.

dramatic increase over naive expectations for momenta in excess of, say, 300 or 400 MeV/c when short-range correlations are included [49,50]).

There are other models [36,51]) which involve scattering from a few-nucleon cluster, but in these models the observed proton in the (p, p′) reaction is the incident proton, it having undergone a large momentum transfer collision and rebounded out of the nucleus. It is not clear whether these models can explain reactions related to (p, p′), namely, (p, n) and (γ, p), so they will be discussed below only in passing.

Shown in fig. 15 are the kinematic labels for the direct knockout model. When the direct knockout model was first applied to wide-angle (p, p′) data, it was assumed for simplicity that the recoil system was in fact a single coherent state. This assumption, which would imply that the momenta of the forward protons in the (p, 2p) experiment would be confined to a line in figs. 11 and 12 (rather than a section of the plane), is obviously not supported by this experiment. However, other calculations [17]) involving only inclusive processes also reached this conclusion: a calculation of the (γ, p) reaction (with bremsstrahlung photons) using parameters determined from the (p, p′) reaction gave their best agreement when the coherent-recoil assumption was dropped and it was assumed that there was a distribution

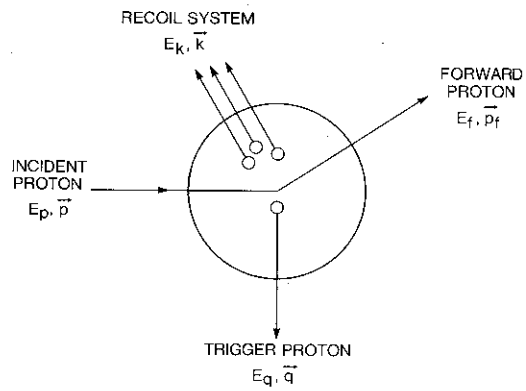

Fig. 15. Kinematic labels used in the direct knockout model.

of the invariant mass of the recoil system. We will compare our (p, 2p) results with this calculation.

The parametrization chosen for the $(\gamma, \mathrm{p})/(\mathrm{p}, \mathrm{p}')$ analysis was the following. The cross section was expressed as [17])

$$\frac{\mathrm{d}^3\sigma}{\mathrm{d}^3q} = \frac{1}{2^4(2\pi)^5 pW_q} \sum_{i=1}^{A_T-1} \frac{a_i(i+1)}{M_{T_i}} \int \frac{\mathrm{d}^3p_f}{W_f} \mathrm{d}^4K D_i(K) n(k) (Z_T|T_{pp}|^2 + N_T|T_{pn}|^2)$$
$$\times \delta^4(\text{energy-momentum}), \tag{7}$$

where K is the total four-momentum of the recoiling i-nucleon jet (k is the three momentum), W_x is the total energy of particle x, and

$$D_i(K) = \frac{1}{2\sqrt{\pi}\eta_i \mathcal{M}_i(K)} \exp\left[-\left(\frac{\mathcal{M}_i(k) - \mathcal{M}_i^0}{\eta_i}\right)^2\right] \tag{8}$$

are the recoiling jet invariant mass distributions. This form was chosen so that the distribution became a delta function in the limit that $\eta_i \to 0$. The widths η_i were taken to be i times η_0, where $\eta_0 \equiv 15$ MeV. The number of protons and neutrons in the target is Z_T and N_T respectively. The quantity T is the elementary nucleon–nucleon transition matrix element evaluated at t or $u = (p - p_f)^2$ for T_{pp} and T_{pn}, respectively. The remaining dependence of the cross section on the kinematical variables is summarized in the structure function $n(k)$. In the plane-wave impulse approximation (PWIA) picture, $n(k)$ is the single-nucleon inclusive momentum distribution, and is only a function of k. Although this model is more general than PWIA, we still assume that n is only a function of k.

We will introduce two parameters g and k_0 into the weighting factor, a_i, and $n(k)$ respectively, namely

$$a_i = g^{i-1}, \tag{9}$$

$$n(k) = \frac{C}{[2\cosh(k/2k_0)]^2} \equiv CF(k)\,. \tag{10}$$

The normalization constant C is determined by the approximate normalization condition

$$A_{\mathrm{T}} = \frac{C\int F(k)\,\mathrm{d}^3k\,\sum_{i=1}^{A_{\mathrm{T}}-1} a_i}{2(2\pi)^3 M_{\mathrm{B}}}\,, \tag{11}$$

where M_{B} is the average mass of a bound nucleon (which we take to be 931.5 MeV). The parameters g and k_0 were determined by fitting $T_{\mathrm{p}} = 800$ MeV (p, p′) data [33]) for light targets to be $g = 0.9$ and $k_0 = 120$ MeV/c with η_0 fixed at 15 MeV. The results were not very sensitive to η_0. An approximation had to be made to eq. (7) in order to obtain a one-dimensional numerical integral over the invariant mass distribution which was simple to evaluate. The reader is referred to ref. [17]) for details, the only point which we wish to make here being that not only will the quoted values of g and k_0 contain some uncertainty from the fitting procedure, but there will also be an error from the approximations used. These values of the parameters also did a reasonable job of reproducing the data at 6 and 400 GeV incident proton energy.

Returning to the expression to be evaluated, one can see that the $\boldsymbol{p}_{\mathrm{f}}$ integration can be done trivially by integrating over the momentum-conserving δ-function. Let us assume that $|T|^2$ is a slowly varying function of k [which it should be at 300 MeV incident energy [52]), but is not at 800 MeV, necessitating a different approximation procedure here from that used in ref. [17])]. Defining θ_k and ϕ_k as the polar angles of $\boldsymbol{k}$ with respect to the $\boldsymbol{p}-\boldsymbol{q}$ axis, then the integrand is independent of ϕ_k in this approximation and it can be integrated out to give 2π. The θ_k integral is removed via the energy-conserving delta function to yield

$$\frac{\mathrm{d}^3\sigma}{\mathrm{d}^3q} = \frac{1}{2^4(2\pi)^4 p W_q|\boldsymbol{p}-\boldsymbol{q}|}\sum_i \frac{a_i(i+1)}{M_{\mathrm{T}_i}}\int \mathcal{M}_k\,\mathrm{d}\mathcal{M}_k \int \frac{k\,\mathrm{d}k}{W_k} D_i(\mathcal{M}_k)n(k)$$
$$\times(Z_{\mathrm{T}}|T_{\mathrm{pp}}|^2 + N_{\mathrm{T}}|T_{\mathrm{pn}}|^2)\,. \tag{12}$$

For the large values of k that are relevant here, $n(k)$ can be approximated by

$$n(k) = C\exp(-k/k_0)\,, \tag{13}$$

and the integral over k can be done analytically:

$$\int_{k_{\min}}^{k_{\max}} Ck\exp(-k/k_0)\,\mathrm{d}k = Ck_0(k+k_0)\exp(-k/k_0)\Big|_{k_{\max}}^{k_{\min}}\,. \tag{14}$$

This leaves one integral to perform numerically, the integral over the invariant mass which we perform using Simpson's rule. The transition matrix element is

related to the pp elastic differential cross section, the normalization chosen here being

$$\frac{d\sigma}{dt} = \frac{|T_{pp}|^2}{64\pi p_{c.m.}^2 s}, \tag{15}$$

where $p_{c.m.}$ is the centre-of-mass momentum and s and t are the usual Mandelstam variables. This can be parametrized as [52])

$$\frac{d\sigma}{dt} = \left.\frac{d\sigma}{dt}\right|_{t=0} e^{bt}, \tag{16}$$

where $b = 0.35\ \mathrm{GeV}^{-2}$ and $d\sigma/dt(t=0) = 87.5\ \mathrm{mb/GeV}^2$ at these energies. Similarly, the p + n charge-exchange cross section we parametrize as

$$\frac{d\sigma}{du} = \left.\frac{d\sigma}{du}\right|_{u=0} e^{b'u} \tag{17}$$

with $b' = 7.7\ \mathrm{GeV}^{-2}$ and $d\sigma/du(u=0) = 122\ \mathrm{mb/GeV}^2$.

One finds that only very slight changes to the parameters determined from 800 MeV data are required to reproduce the 300 MeV data. The smooth curves shown on fig. 1 are the results of this calculation with $g = 0.9$ and $\eta_0 = 15$ MeV, as before, but k_0 now raised slightly to 125 MeV/c. The quality of the fit is obviously very good. We did not attempt a fit to the 40° or 60° data because the approximations used here will not be valid in the quasifree region, and a calculation at forward angles would have to sum over the incident proton as well as protons knocked out of the nucleus. Indeed, naive application of eq. (12) at forward angles underpredicts the data by about a factor of two, as one would expect.

We have gone through the details of the inclusive cross-section calculation because the coincidence calculation can be found from it very easily by simply removing the d^3p_f integral from the r.h.s. of eq. (7) and integrating out d^4K using the four-dimensional δ-function to obtain

$$\frac{d^6\sigma}{d^3q\, d^3p_f} = \frac{1}{2^4(2\pi)^5 p W_q W_f} \sum_{i=1}^{A_T-1} \frac{a_i(i+1)}{M_{T_i}} D_i(K) n(k) Z |T_{pp}|^2 \tag{18}$$

for the (p, 2p) reaction.

The predictions of this expression for trigger proton energies of 70 and 110 MeV are shown in figs. 16 and 17, respectively. In each figure, the differential multiplicities at fixed forward-proton angle and variable energy are shown for three different forward angles. One can see that the model predictions follow the general behavior of the data as a function of forward angle and energy, and trigger energy. The ragged behavior is due to the thresholds in the sum over the recoiling jets. However, the predictions are typically a factor of two too large. This may reflect a calculational effect in that

(i) the model may be overpredicting the high energy end of the energy spectrum but underpredicting the low-energy end, and

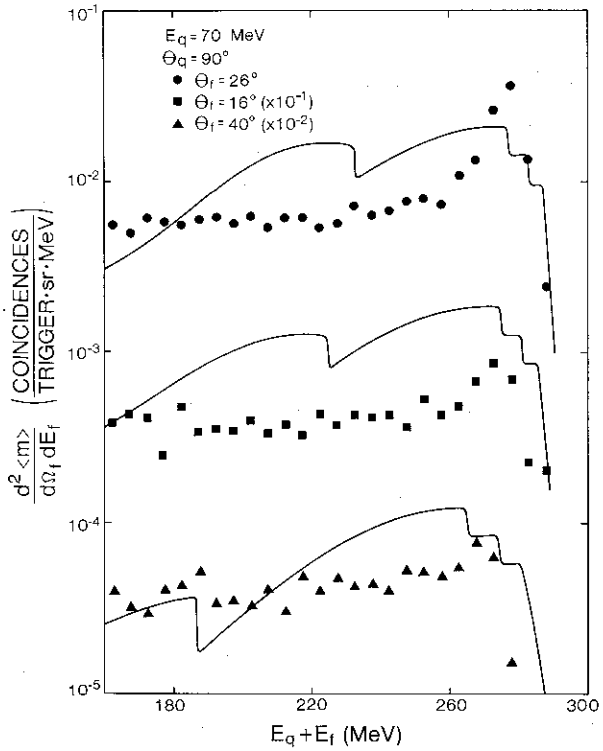

Fig. 16. Comparison of the direct knockout model [ref. [17])] predictions for the differential multiplicity at $E_q = 70$ MeV and $\theta_f = 16, 26$, and 40°.

(ii) the model has not taken into account the fact that the outgoing forward proton may charge exchange to emerge from the target as a neutron, thus resulting in an overprediction of the coincidence rate.

However, the disagreement may also be an indication that only on the order $\frac{1}{3}$ to $\frac{1}{2}$ of the inclusive events have a direct knockout origin, the rest being attributable to other mechanisms.

To summarize this calculation, a functional form was assumed for the distribution of the invariant mass of the recoil system in the direct knockout model, and the parameters of this function were determined by fitting the (γ, p) and (p, p') cross sections at intermediate energies. This functional form did not include any allowance for near coherent enhancements, such as those observed in fig. 11, since the (γ, p) fits would not have been sensitive to their presence. Rather, what the (γ, p) and (p, p') can be used for is estimating the "continuum" part of the invariant mass distribution. Considering the uncertainties in the method of determining this distribution, since the procedure measures the integral of the distribution and not the

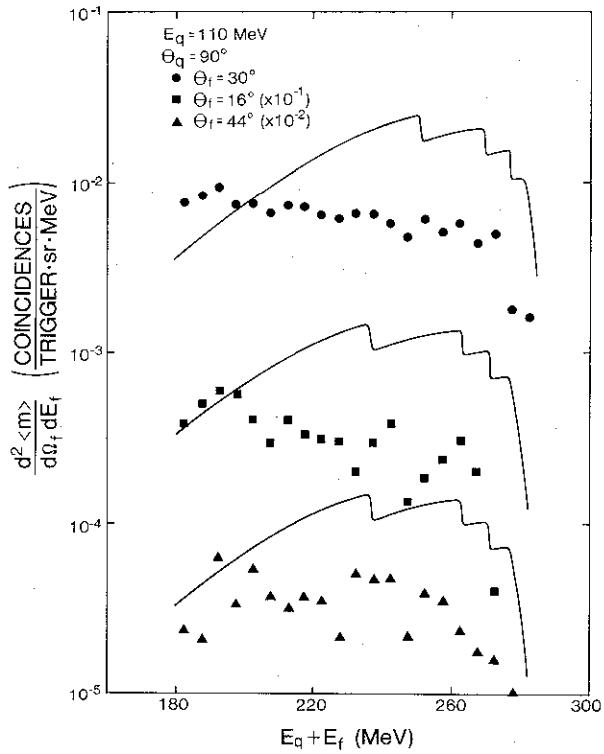

Fig. 17. Comparison of the direct knockout model [ref. [17]] predictions for the differential multiplicity at $E_q = 110$ MeV and $\theta_f = 16$, 30, and 44°.

distribution itself, the agreement of the shape and normalization of the predicted energy spectra with the data is encouragingly good.

One observation which is worth commenting on from figs. 11 and 12 is the peaking of the differential multiplicity as a function of forward-proton angle. One can see that in both cases, the peaking is at a slightly larger angle (with respect to the beam) than the angle for minimum residual system recoil momentum, often called the QTBS angle. Looking at eq. (18) for a moment, the function $n(k)$ will have the strongest angular dependence and will be peaked at the smallest value of k, which occurs along the $\boldsymbol{p} - \boldsymbol{q}$ direction. Clearly then, one would expect to find the peak in the differential cross section near to the QTBS angle. Including the angular dependence of $|T_{pp}|^2$ in eq. (18) will move the peak to smaller angles [see ref. [41]]. This functional form will not give peaking even at the few degrees outside the QTBS angle at which it is observed. This observation of larger than QTBS peaking was also seen in the 800 MeV experiment [4]), and so it is probably not an artifact of this experiment. Its origin very likely lies with the multiple scattering of the projectile or ejectile. We will give several examples showing how multiple scattering will shift the peak of the forward proton to wide angles. For convenience,

we will use a numerical example in which the trigger proton is observed at 90° with a kinetic energy of 70 MeV, for which the QTBS angle is 24.6°. We require that the peak shift outwards by about 3°. Some mechanisms are:

(i) The trigger proton was originally scattered into a more forward direction but with the same energy. Because the inclusive cross sections are strongly forward peaked, multiple scattering will tend to spread the events to wider angles. For our numerical example the maximum shift in the QTBS angle which could be produced by this mechanism (~2.6°) would require that the trigger proton would have to be scattered originally to about 63°.

(ii) The incident proton had lost kinetic energy because of multiple scattering, before the interaction with the trigger proton. This would result in an increase in the QTBS angle. However, the decrease in energy required is perhaps a little large if this mechanism alone is to account for the shift: in our example, to produce a QTBS angle of 28°, the incident proton would have to have lost about 70 MeV. This is not consistent with the downward shift in forward-proton energy of the peak: no more than approximately 25 MeV.

(iii) The trigger proton was scattered at 90° but had a larger energy. Multiple scattering then reduced its energy as it emerged from the nucleus. In our numerical example, the struck proton would have to have been given an extra 20 MeV of kinetic energy in order to shift the QTBS angle by 3°.

As usual with inclusive reactions, the real mechanism is probably a combination of the above possibilities, each giving a small contribution. As an example of the difficulties encountered with explanations relying on a single mechanism let us consider, as a model, mechanism (i) in the extreme that the coincidence events are multiple quasifree scatterings. A similar model has been considered for the 800 MeV results [6]). Let us consider the trigger energy dependence of this model. The angle of 63° quoted in the numerical example for mechanism (i) corresponds to quasifree scattering. As the trigger proton energy increases, so does the quasifree angle of the forward partner. In fact the difference between the quasifree angle and the QTBS angle also increases with energy. For example, for a trigger energy of 150 MeV, the difference between the quasifree angle of the forward proton and the QTBS angle is more than 8°, in contrast with the 2.6° calculated at a 70 MeV trigger energy. However, this behavior is not what is observed in the present experiment, as shown in fig. 10. Here, it is observed that the maximum in the differential multiplicity moves toward the QTBS angle, not away from it, with increasing trigger energy. Hence, the extreme version of mechanism (i) cannot be the only contributor to the shift in the coincidence rate peak.

5. Summary and conclusions

This paper has reported measurements of the differential mean multiplicity (coincidences/trigger · sr · MeV) of coplanar companion protons associated with

trigger protons scattered at 90° from a beam of 300 MeV protons incident on a ^{9}Be target. Wide ranges in the values of the trigger proton energy E_q, the associated proton energy E_f, and the angle θ_f have been examined. In our data we find no particular enhancements which may be associated with processes emphasized by the limited kinematic regime chosen in refs. [5,7]) for large-angle-triggered (p, 2p) measurements at 640 MeV, nor do we find the ratio of coincidence to forward singles spectra to be independent of angle as reported in ref. [4]) for a limited range of data taken on large-angle-triggered ^{6}Li (p, 2p) processes at 800 MeV.

The data obtained can be conveniently divided into two qualitative classes, namely that for coherent or near-coherent residual system recoil (the CR region) and that associated with significant residual system excitation where the dependence on the summed energy of the two detected protons is found to be slowly varying (the continuum region). Both regions have angular dependences which have maxima at angles ranging from near those for minimum residual system recoil momenta (QTBS angles) to angles somewhat larger than the QTBS angles, the deviation from the QTBS angle being larger for smaller values of the 90° trigger proton energy. The differential mean multiplicity of the CR region decreases rapidly as a function of increasing trigger proton energy while that for the continuum region varies slowly with trigger energy. Integration of the data, assuming symmetry about the angle of maximal differential mean multiplicity, indicates that a substantial fraction of protons scattered at 90° are accompanied by companion protons of 70 MeV or greater energy but that this fraction decreases significantly as the energy of the trigger increases.

In a theoretical analysis of this data, we find evidence which tends to confirm the conclusions drawn about thermal and phase-space models from other inclusive experiments. The hot-spot model analysis of (p, p′) measurements consistently yields a picture in which the incident proton loses its energy to a small cluster of nucleons even for heavy targets. These then come to thermal equilibrium and evaporate nucleons in a statistical fashion. However, we find that a significant fraction of wide-angle energetic protons are accompanied by a fast forward proton highly correlated in angle and which has often lost little more energy than what is required to eject the trigger proton. Such a leading particle effect would not be expected from a hot-spot model. While this does not rule out the hot-spot model as a contributor to the production of wide-angle energetic ejectiles, it does point to another more direct reaction mechanism as being of significance. A coincidence experiment carried out at lower forward proton energies might help to evaluate the relative contributions of hot-spot mechanisms.

Similarly, a comparison was made with a model in which the coincidence rate was proportional to the phase space available to the recoiling system. Again, the data do not support such a description.

The predictions of a direct knockout model which was used in (γ, p) and (p, p′) analyses were compared with the (p, 2p) results. The shape and normalization of

the differential multiplicity can be treated as a measure of the invariant mass distribution of the recoiling system in the direct knockout model. This distribution was determined crudely in a comparison of (γ, p) to (p, p′) differential cross section, and was observed to reproduce the measurements here to within about a factor of 2, encouragingly good agreement considering the method used to determine the distribution. However, it seems unlikely that the direct knockout model can explain the fact that the peak of the angular distribution of forward protons is slightly outside the QTBS angle, unless there is multiple scattering.

This work was supported by the Natural Science and Engineering Research Council of Canada. The authors would like to acknowledge the assistance received from the University of Alberta group at TRIUMF, especially the efforts of D.A. Hutcheon and R. Abegg during the course of the experiments. We wish to thank N. Bohna for her help in processing the data through the Simon Fraser University computing centre and the operations staff of TRIUMF for their efforts in obtaining the proton beams used in this experiment.

References

1) S. Nagamiya and M. Gyulassy, in Advances in nuclear science, ed. J.W. Negele and E.W. Vogt (Plenum, New York, in press) (also available as Lawrence Berkeley Laboratory Report LBL-14035)
2) D.H. Boal, in Proc. Intermediate Energy Nuclear Chemistry Workshop, Los Alamos Report LA-8835-C
3) A.G. Flowers *et al.*, Phys. Rev. Lett. **40** (1978) 709; **43** (1979) 323
4) S. Frankel, W. Frati, C.F. Perdrisat and O.B. Van Dyck, Phys. Rev. **C24** (1981) 2684
5) V.I. Komarov, G.E. Kosarev, H. Müller, D. Netzband, V.D. Toneev, T. Stiehler, S. Tesch, K.K. Gudima and S.G. Mashnik, Nucl. Phys. **A326** (1979) 297
6) S. Frankel and W. Frati, Phys. Rev. **C24** (1981) 2739
7) V.I. Komarov, G.E. Kosarev, H. Müller, D. Netzband, T. Stiehler and S. Tesch, Phys. Lett. **80B** (1978) 30
8) I. Tanihata, Y. Miake, H. Hamagaki, S. Kadota, Y. Shida, R. Lombard, E. Moeller, S. Nagamiya, S. Schnetzer and H. Steiner, in Proc. 5th High Energy Heavy Ion Summer Study, LBL-12652, Conf-8105104, Berkeley, May 1981, p. 365;
see also Y. Miake, University of Tokyo Institute for Nuclear Study report, INS-NUMA-39 (1982)
9) R.E.L. Green and R.G. Korteling, Phys. Rev. **C18** (1978) 311
10) R.E.L. Green and R.G. Korteling, Phys. Rev. **C22** (1980) 1594
11) R.E.L. Green, K.P. Jackson and R.G. Korteling, Phys. Rev. **C25** (1982) 828
12) J.P. Alard, A. Baldit, R. Brun, J.P. Costilhes, J. Dhermain, J. Fargeix, L. Fraysse, J. Pellet, G. Roche, J.C. Tamain, A. Cordaillat and A. Pasinetti, Nuovo Cim. **30A** (1975) 320
13) V.I. Bogatin, V.F. Litvin, O.V. Lozhkin, N.A. Perfilov and Yu.P. Yakovlev, Nucl. Phys. **A260** (1976) 446
14) E.N. Volnin, G.M. Amalsky, D.M. Seleverstov, N.N. Smirnov, A.A. Vorobyov and Yu.P. Yakolev, Phys. Lett. **55B** (1975) 409
15) S. Frankel, W. Frati, O. Van Dyck, R. Werbeck and V. Highland, Phys. Rev. Lett. **36** (1976) 642
16) D.H. Boal and R.M. Woloshyn, Phys. Rev. **C20** (1979) 1878
17) D.H. Boal and R.M. Woloshyn, Phys. Rev. **C23** (1981) 1206
18) D.H. Boal, R.E.L. Green, R.G. Korteling and M. Soroushian, Phys. Rev. **C23** (1981) 2788
19) D.H. Boal and M. Soroushian, Phys. Rev. **C25** (1982) 1003

20) T. Berggren and H. Tyrén, Ann. Rev. Nucl. Sci. **16** (1966) 153
21) G. Jacob and Th.A.J. Maris, Rev. Mod. Phys. **38** (1966) 121; **45** (1973) 6
22) Th.A.J. Maris, M.R. Teodoro and E.A. Veit, Phys. Rev. **C20** (1979) 446
23) A.N. James, W.J. McDonald, J.M. Cameron, C.A. Miller, D.A. Hutcheon, P. Kitching, G.C. Neilson, G.M. Stinson and E.D. Earle, Nucl. Phys. **A324** (1979) 253
24) P. Kitching, C.A. Miller, W.C. Olsen, D.A. Hutcheon, W.J. McDonald and A.W. Stetz, Nucl. Phys. **A340** (1980) 423
25) M.B. Epstein, D.J. Margaziotis, J. Simone, D.K. Hasell, B.K.S. Koene, B.T. Murdoch, W.T.H. van Oers, J.M. Cameron, L.G. Greeniaus, G.A. Moss, J.G. Rogers and A.W. Stetz, Phys. Rev. Lett. **44** (1980) 20
26) L. Antonuk, P. Kitching, C.A. Miller, D.A. Hutcheon, W.J. McDonald, G.C. Neilson, W.C. Olsen and A.W. Stetz, Nucl. Phys. **A370** (1981) 389
27) C.A. Goulding and J.G. Rogers, Nucl. Instr. **153** (1978) 511
28) J.M. Cameron, P. Kitching, R.H. McCamis, C.A. Miller, G.A. Moss, J.G. Rogers, G. Roy, A.W. Stetz, C.A. Goulding and W.T.H. van Oers, Nucl. Instr. **143** (1977) 399
29) R.E. Chrien, T.J. Krieger, R.J. Sutter, M. May, H. Palevsky, R.L. Stearns, T. Kozlowski and T. Bauer, Phys. Rev. **C21** (1980) 1014
30) S. Frankel. Phys. Rev. Lett. **38** (1977) 1338
31) S. Frankel, Phys. Rev. **C17** (1978) 694
32) S. Frankel, W. Frati. M. Gazzaly, G.W. Hoffmann, O. Van Dyck, and R.M. Woloshyn, Phys. Rev. Lett. **41** (1978) 148
33) S. Frankel, W. Frati, G. Blanpied, G.W. Hoffmann, T. Kozlowski, C. Morris, H.A. Thiessen, O. Van Dyck, R. Ridge and C. Whitten, Phys. Rev. **C18** (1978) 1375
34) J. Källne, A.W. Stetz and R.M. Woloshyn, Phys. Lett. **74B** (1978) 170
35) R.D. Amado and R.M. Woloshyn, Phys. Rev. Lett. **36** (1976) 1435
36) T. Fujita, Phys. Rev. Lett. **39** (1977) 174
37) H.J. Weber and L.D. Miller, Phys. Rev. **C16** (1977) 726
38) R.M. Woloshyn, Nucl. Phys. **A306** (1978) 333
39) S.T. Thornton, K.R. Cordell, L.C. Dennis, R.R. Doering and T.C. Schweizer, Phys. Rev. **C19** (1979) 913
40) S. Nagamiya, L. Anderson, W. Brückner, O. Chamberlain, M.-C. Lemaire, S. Schnetzer, G. Shapiro, H. Steiner and I. Tanihata, Phys. Lett. **81B** (1979) 147
41) D.H. Boal, Phys. Rev. **C21** (1980) 1913
42) D.H. Boal, in Proc. Relativisitic Heavy Ion Winter School, Banff, 1982 (unpublished), available as TRIUMF report TRI-PP-82-7
43) G. Roy, L.G. Greeniaus, G.A. Moss, D.A. Hutcheon, R. Liljestrand, R.M. Woloshyn, D.H. Boal, A.W. Stetz, K. Aniol, A. Willis, N. Willis and R. McCamis, Phys. Rev. **C23** (1981) 1671
44) B.D. Anderson, A.R. Baldwin, A.M. Kalenda, R. Madey, J.W. Watson, C.C. Chang, H.D. Holmgren, R.W. Koontz and J.R. Wu, Phys. Rev. Lett. **46** (1981) 226
45) D.H. Boal, Phys. Rev. **C25** (1982) 3068
46) R. Weiner and M. Weström, Phys. Rev. Lett. **34** (1975) 1523
47) J. Knoll, Phys. Rev. **C20** (1979) 773
48) E. Byckling and K. Kajantie, Particle kinematics (Wiley, London, 1973)
49) J.G. Zabolitzky and W. Ey, Phys. Lett. **76B** (1978) 527
50) J.W. Van Orden, W. Treux and M.K. Banerjee, Phys. Rev. **C21** (1980) 2628
51) S.A. Gurvitz, Phys. Rev. **C22** (1980) 964, and references therein
52) Particle Data Group, NN and ND interactions (above 0.5 GeV/c)—a compilation (Lawrence Radiation Laboratory, Berkeley, 1970)